Word count: 5235

Development of one-part geopolymers for 3D concrete printing

Biranchi Panda[1], GVP Bhagath Singh[2], Cise Unluer[2*], Ming Jen Tan[1]

[1]Singapore Centre for 3D Printing, School of Mechanical & Aerospace Engineering
Nanyang Technological University, 50 Nanyang Avenue, Singapore 639798
[2] School of Civil and Environmental Engineering, Nanyang Technological University, 50 Nanyang Avenue, Singapore 639798
* Corresponding author. Tel.: +65 91964970, E-mail address: ucise@ntu.edu.sg

Abstract:

Interest in innovative construction processes such as 3D concrete printing (i.e. digital construction), is growing rapidly both in academia and industry. Processing conventional geopolymer mixes, in which alkaline solutions are used for activation, could be troublesome in concrete printing due to the high viscosity of the alkaline solution. One-part geopolymers offer one possible solution to this challenge as they involve the use of a solid activator with solid aluminosilicates precursors. In this work, a printable one-part geopolymer mix was developed, which could be extruded through the nozzle of a 3D printer and stacked together without deforming the bottom layers. Flow properties such as yield stress, viscosity and thixotropy of the developed geopolymer were assessed along with its strength development curve. Printed specimen showed anisotropic behaviour in mechanical properties when compared to the mould casted samples. Microstructural characterization revealed the formation of alumino-silicate gel with high tetrahedrally coordinated Al and interlayer K ions in its structure. When compared to OPC-based mixes, the developed geopolymer mixes revealed a lower environmental impact, which could be even further reduced with the use of alternative activators.

Keywords: Digital construction; rheology; one-part geopolymer; mechanical properties; environmental assessment

1. Introduction

The increasing demand for environmentally friendly and sustainable construction materials has necessitated the identification of alternative materials for ordinary Portland cement (OPC). In this regard, geopolymer cement, involving the use of various industrial wastes and by-products, has the potential to be considered as a promising alternative to OPC in certain applications. The term "geopolymer" was first introduced in the literature in 1978, characterizing a new class of materials with the ability to poly-condense at low temperatures like "polymers" [1]. This process involves the chemical reaction of aluminosilicate materials (e.g. fly ash, metakaolin, granulated blast furnace slag and silica fume) with Na- or K-based alkali activators. When mixed with the alkaline activators, setting and hardening take place, yielding a material with good binding properties. Several advantages of geopolymer materials over OPC, namely potential environmental benefits, high compressive strength, rapid controllable setting and hardening, fire resistance, and acid and salt solution resistance have been reported [2]. Despite the remarkable potential of geopolymers, the conventional two-part mixing process presents challenges in their scalability due to handling issues and viscosity of the alkaline solution. Therefore, one-part geopolymers, which are mixtures of a solid alkaline activator and an aluminosilicate precursor, can be used to solve some of these shortcomings [3, 4].

Different synthesis routes in designing one-part geopolymer cements, either by activating aluminosilicates together with alkalis at elevated temperatures or blending the aluminosilicates with solid activators, have been reported [5, 6]. A recent review of these techniques [7] provided a summary of the potential benefits, environmental impacts and cost of one-part systems. Nevertheless, the use of one-part geopolymers in concrete printing/digital construction, which is gaining significant attention both in academia and the construction practice [8-10], has not been discussed in detail until now. Most of the work presented in this area so far has focused on exploring the material properties required for 3D printing involving the use of OPC-based binders, with and without the use of fibers [11-13]. Within this context, parameters such as extrudability, shape retention, open time and buildability properties, collectively described as "printability" that refers to the layer-by-layer deposition of cementitious mortars according to a CAD model [14], need to be studied further.

Building materials with a high yield strength and low viscosity are usually preferred in concrete printing, where the yield stress is linked to the shape retention and buildability characteristics and viscosity is an indication of the ease of mortar extrusion. The main challenge exists in controlling the structuration rate of the material without disturbing its flow properties so that the well extruded layers can be deposited in a layer-by-layer manner. Due to the thixotropic nature of OPC particles [15], it is possible to achieve printable properties, during which the material can flow smoothly via the applied shear force and can incrementally gain yield stress by particle interaction/flocculation at rest. Although the use of two-part systems has been studied previously [16, 17], where a 60-cm tall structure using fly ash and slag-based geopolymers was printed [17], no detailed studies on the use of one-part geopolymers in 3D printing have been reported until now. Therefore, this paper aims to study the formulation of one-part geopolymers and provide an assessment of their fresh properties (e.g. yield stress, viscosity and thixotropy) to evaluate their suitability in non-structural concrete printing applications. Furthermore, the mechanical performance of the printed sections was tested in compression after 28 days of ambient curing and their directional properties were compared with mould casted geopolymers. The strength and microstructural development of the prepared formulations was further supported by an investigation and quantification of the phase formations via x-ray diffraction (XRD) and field emission scanning electron microscopy (FESEM) analyses. The energy and CO_2 emissions associated with one-part geopolymer mixes were also provided to evaluate their potential against OPC from an environmental standpoint.

2. Materials and Methodology

2.1 Materials

Class F grade fly ash (FA), conforming to ASTM C 618, was obtained from Thermal Powertech Corporation Ltd. (India). Ground granulated blast furnace slag (GGBS) was supplied by EnGro Corporation Ltd. (Singapore). Table 1 shows the chemical compositions of FA and GGBS, obtained via X-ray fluorescence (XRF) analysis.

Table 1. Chemical compositions (%) of FA and GGBS

Material	SiO_2	CaO	Al_2O_3	Fe_2O_3	SO_3	MgO	Na_2O	K_2O	TiO_2	LOI
FA	51.1	5.8	28.8	6.4	1.0	1.1	0.3	1.2	2.5	1.2
GGBS	29.6	39.3	15.5	0.3	4.3	7.5	0.4	0.5	1.7	1.1

As can be seen from Fig. 1, both FA and GGBS contained different crystalline phases along with broad humps that represented the amorphous phases present in each material. FA mainly consisted of quartz (PDF# 074-3485) and mullite (PDF# 074-4143) in crystalline form, whereas GGBS displayed a broad amorphous hump at around 30° 2θ and gehlenite (PDF#0 04-0690), which was present in small amounts.

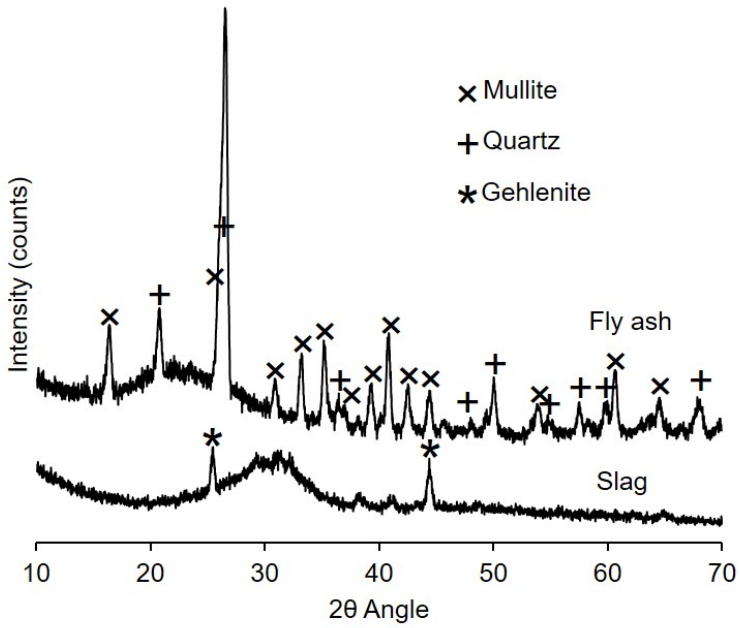

Fig. 1 X-ray diffractograms of FA and GGBS

The glassy contents of FA and GGBS were determined using an external standard approach, as outlined in [21]. Results shown in Table 2 revealed that FA contained a low amount of reactive phases, which could be due to usage of low grade coal and low ignition temperatures [22].

Table 2. Reactive components of FA and GGBS

Material	Crystalline content (%)						Amorphous content (%)
	Al_2O_3	SiO_2	Fe_2O_3	CaO	K_2O	TiO_2	
FA	10.72	14.28	5.94	2.75	2.17	1.47	38.8
GGBS			2.8				97.2

Other than FA and GGBS, the alkaline activator used in this study was formulated by blending potassium silicate powder (32.4 wt.% SiO_2, 13.5 wt.% Na_2O and 54.1 wt.% H_2O) together with potassium hydroxide (KOH) powder to reach the desired modulus of 1.5 [23]. For the preparation of geopolymer mortars, fine river sand with a max particle size of 2 mm was used along with tap water.

2.2 Sample preparation

Five geopolymer mortars with a constant water/solid (i.e. solid component consisting of FA, GGBS and anhydrous activator) ratio of 0.35 were prepared by varying the GGBS and activator contents, as shown in Table 3. Accordingly, the GGBS (G) ranged between 15-40% of the overall binder (FA+GGBS) content within samples F85G15A15, F70G30A15 and F60G40A15, in which the activator (A) content was kept constant at 15% (i.e. by mass) of the binder. Furthermore, the FA and GGBS contents remained constant, whereas the activator dosage varied at 10, 15 and 20% in samples F70G30A10, F70G30A15 and F70G30A20, respectively. For the preparation of mortar samples, fine river sand was added to the binder at a sand/binder ratio of 0.85, along with the activator and mixed for two minutes in a Hobart planetary mixer. This was followed with the addition of the required amount of water into the mixing bowl, after which mixing continued until a homogeneous mixture was obtained.

Table 3. Mix proportions of one-part geopolymer mixes prepared in this study

Mix name	Binder composition (wt.%)		Activator content (%)
	FA	GGBS	
F85G15A15	85	15	

F70G30A15	70	30	15
F60G40A15	60	40	
F70G30A10	70	30	10
F70G30A20	70	30	20

2.3 Methodology

2.3.1 Process overview of 3D concrete printing

3D concrete printing is similar to other 3D printing processes, where the model is first designed in CAD platform, followed by slicing and G-code generation [18]. The G-code is later interpreted by a controller that sends commands to either an industrial robot or gantry printer, connected to a concrete pump and extruder/nozzle. Fig. 2 shows the steps involved in a typical concrete printing process, during which the fresh material is deposited layer-by-layer via a 4-axis industrial robot.

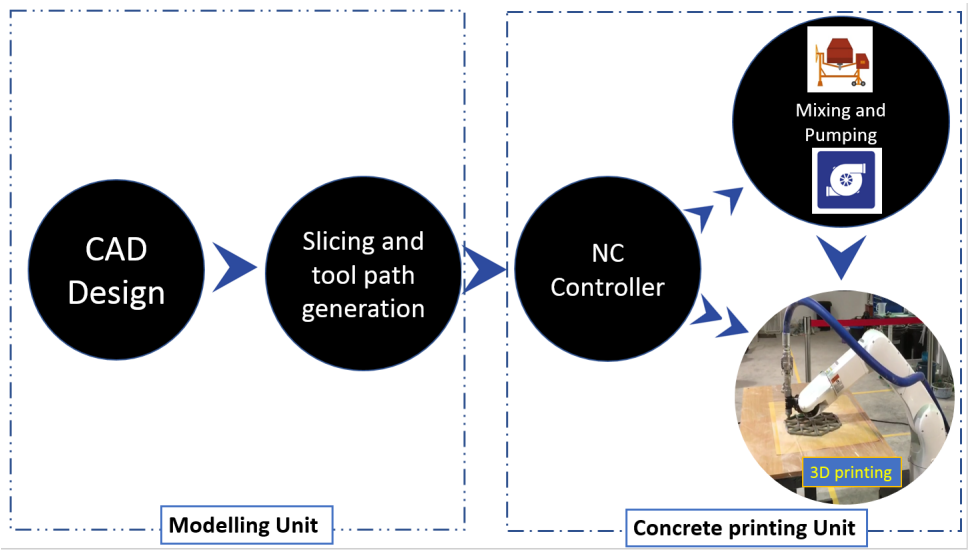

Fig. 2 Steps involved in the 3D concrete printing process

During printing, process parameters (e.g. printing speed and layer height), material properties (e.g. rheology and thixotropy) as well as the digital design parameters (e.g. shape and size) play an

important role in determining the quality of the printed filament [19, 20]. These factors are depicted in Fig. 3, which outlines the main parameters controlling the properties of 3D printed concrete.

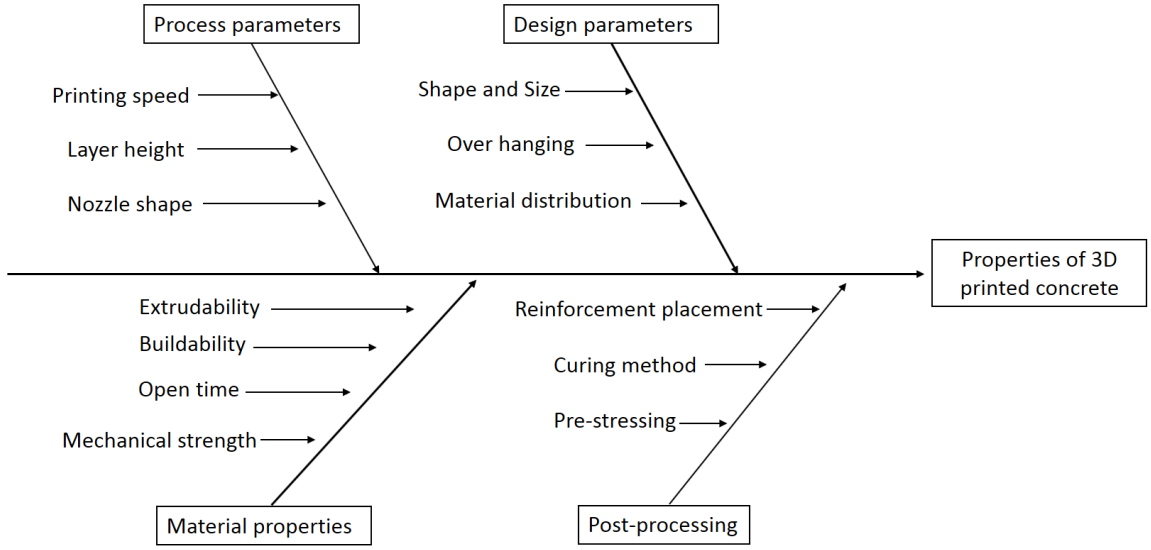

Fig. 3 Cause-effect diagram reflecting the main parameters controlling the properties of 3D printed concrete

2.3.2 Experimental methodology

2.3.2.1 Flow properties

To obtain the evolution of static yield stress, stress growth test was performed by applying deformation at a constant shear rate of 0.1 s^{-1}. During this test, the shear stress progressively developed to a maximum value and then stabilized at an equilibrium value. The static yield stress was defined as the peak shear stress value [25].

2.3.2.2 Thixotropy and viscosity recovery

In this study, thixotropy was measured according to a simplified stress decay model [25], as shown in Equation 1, where τ_e and τ_i are the equilibrium stress and initial shear stress, respectively; α is a constant value; γ is the applied constant shear rate; and t is the shearing time. The thixotropy index (A_{thix}) is defined as the ratio of τ_i and τ_e, indicating the relationship between static and dynamic yield stress, which is critical in 3D concrete printing applications (i.e. the higher the thixotropic index, the higher the thixotropy).

$$\tau = \tau_e + (\tau_i - \tau_e)e^{-\alpha\gamma t} \quad (1)$$

In addition to thixotropy, viscosity recovery is also an important property of printable concrete, which indicates fresh material behaviour after the extrusion process. If the original viscosity of the initial deposited layer is not recovered before the deposition of the second layer, it may result in the deformation of the structure. Therefore, in this study, the 3D printing process was mimicked by applying different shear rates of (i) 0.01 s^{-1} for 60 seconds, (ii) 300 s^{-1} for 30 seconds and (iii) 0.01 s^{-1} for 60 seconds at three different time intervals corresponding to the material state (i) initially at rest, (ii) shearing/extrusion and (iii) again at rest, as used in previous studies [17, 19]. The apparent viscosities were measured during these three intervals to understand the recovery behaviour of the different geopolymer mixes.

2.3.2.3 Compressive strength

To study the hardened properties of the prepared formulations, specimens were cast in 50x50x50 mm moulds and cured under ambient conditions for up to 28 days. Average compressive strengths were measured by uni-axial loading in triplicates, in accordance with the specifications of ASTM C109 [27]. The equipment used for this purpose was a Toni Technik Baustoffprüfsysteme machine, operated at a loading rate of 100 kN/min.

2.3.2.4 3D concrete printing

One of the mixes that met the minimum requirement of M25 grade concrete was selected out of the initially prepared five mix designs and printed using a 4-axis gantry printer fitted with a 40x10 mm rectangular nozzle and a grout pump, and operated at a printing speed of 90 mm/sec. The outcome was a solid printed block with a length of 400 mm. The printed block was then split into 40x40 mm cubes for directional compression testing. The same mix was also cast separately to compare its performance with those extracted from the 3D printed section.

2.3.2.5 Structural build up (load bearing capacity)

The assessment of structural build-up is important for concrete printing since the buildability property depends on the structuration rate of the material (i.e. how fast the material can gain stiffness) after extrusion. Accordingly, the early (i.e. green) strength of the material was measured in the dormant period via the incremental loading of the fresh mortar using an Instron tensile test series machine [28]. These results were further supported with the 28-day hardened properties to analyse the full-strength development of the material.

2.3.2.6 Microstructural characterization (XRD and FESEM)

X-ray diffraction (XRD) and field emission electron microscopy (FESEM) were used to characterize the raw materials and the reaction products of the prepared mixes. Randomly oriented powder samples were extracted from the selected mixes by grinding the dried samples for XRD analysis. The scan patterns were obtained from 10° to 70° 2θ with a step size of 0.02° by using an Empyrean X-ray Diffractometer with Cu-Kα-radiation. The X-ray tube generator was operated at 40 kV and 40 mA. Corundum was used as the external standard for the quantification of both crystalline and amorphous phases using TOPAS software. The crystalline phases were identified using the powder diffraction file-2 [22], while known phases were taken from the ICSD data base. For FESEM analysis, a JEOL JSM-7600F electron microscope, equipped with an energy dispersive analyser was used to examine the sample microstructure after 28 days of curing.

3. Results and Discussion

3.1 Flow and mechanical properties

Fig. 4(a) shows the static yield stress and apparent viscosity of the five mixes containing different GGBS and activator contents. An increase in the GGBS content led to an increase in both the yield stress and viscosity, which could be due to the chemical composition (i.e. presence of calcium) in GGBS and its angular particle shape. Angular particles can provide an interlocking effect, which can increase the yield stress. A similar outcome on the effect of the angular morphology of GGBS on concrete workability was reported in previous studies [29, 30]. Therefore, the partial replacement of 40% of FA with GGBS resulted in 125% increment in the yield stress, which can be useful in the shape fidelity and buildability of the printed layers. As the addition of GGBS was reported to decrease the setting time of alkali-activated materials [29], it can significantly affect the workability time (i.e. open time) by changing the flow properties. Therefore, the amount of GGBS included in these mixes should be carefully controlled with proper activator dosage for the 3D printing of one-part geopolymer mortars. Similarly, increasing the activator content from 10% to 20% in mix F70G30A20 led to a higher yield stress, in line with the findings of [31]. Accordingly, a higher dosage of the activator induced a higher pH and ionic strength of surface charges, which can be related to the increase in the yield stress. The viscosities of geopolymer mortars, irrespective of different slag and activator contents, was found to be substantially low (< 10 Pa·s) under a high shear force. Such unique property (i.e. high yield stress and low viscosity) could find an application in the 3D printing process with some additional attention on thixotropy and structural build-up. The observed decrease in viscosity with increasing shear rate can be attributed to the deflocculating phenomena in the early stages of the alkali-activation process, for which, further mixing can increase the workability of the mixtures before its application.

Similar to the flow properties, the compressive strength of the prepared samples increased with increasing GGBS content, as can be seen in Fig. 4(b). This increase in strength could be attributed to the early formation of C–S–H gel in the matrix [32, 33]. A similar increase was observed with an increase in the activator content from 10 to 20%, which could be due to the presence of a higher

amount of Si ions available for geopolymerisation. This finding was in line with the findings of previous studies [24], where an improvement in strength with respect to the activator (i.e. sodium silicate) content was reported.

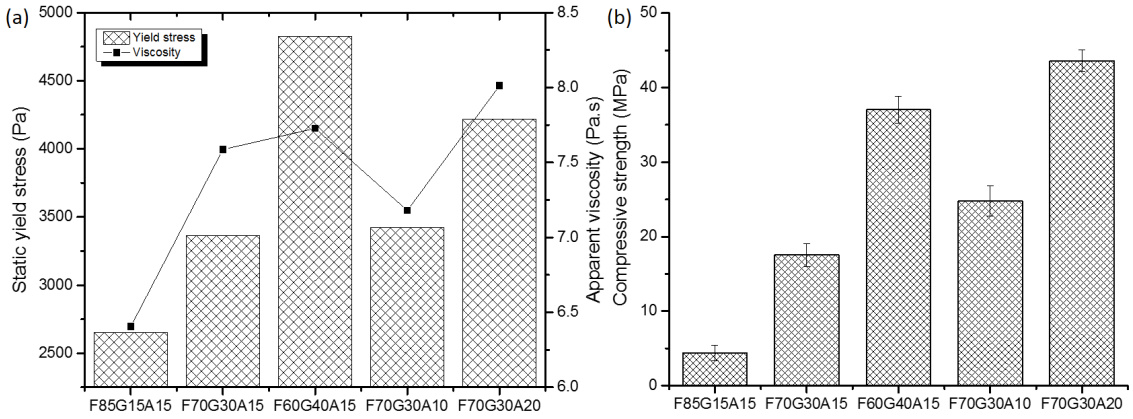

Fig. 4 Assessment of the prepared mixes for their (a) static yield stress and viscosity and (b) compressive strength

Besides the yield stress and viscosity [34], the thixotropy, referring to the reversible structural breakdown and build-up aspect of printable materials, was studied. Throughout this assessment, the continuous decrease of apparent viscosity with time under shear and subsequent recovery at rest was observed. Fig. 5(a) shows the viscosity recovery of each mix, where their recovery ability after being sheared at a shear rate of 300 s^{-1} was revealed. Considering the shear-thinning property of one-part geopolymers (Fig. 5(b)), the patterns observed in viscosity recovery can be linked to the concrete printing process, indicating the properties of each mix after their extrusion from the nozzle. Theoretically, if a material can recover its initial viscosity after the extrusion process, it can maintain its shape without any significant deformation. The findings reported in this study showed that the prepared mixes were able to recover 70-80% of their original viscosity within 60 seconds of extrusion, thereby enabling the deposition of a second layer within the 60 seconds time interval, without deforming the bottom layers.

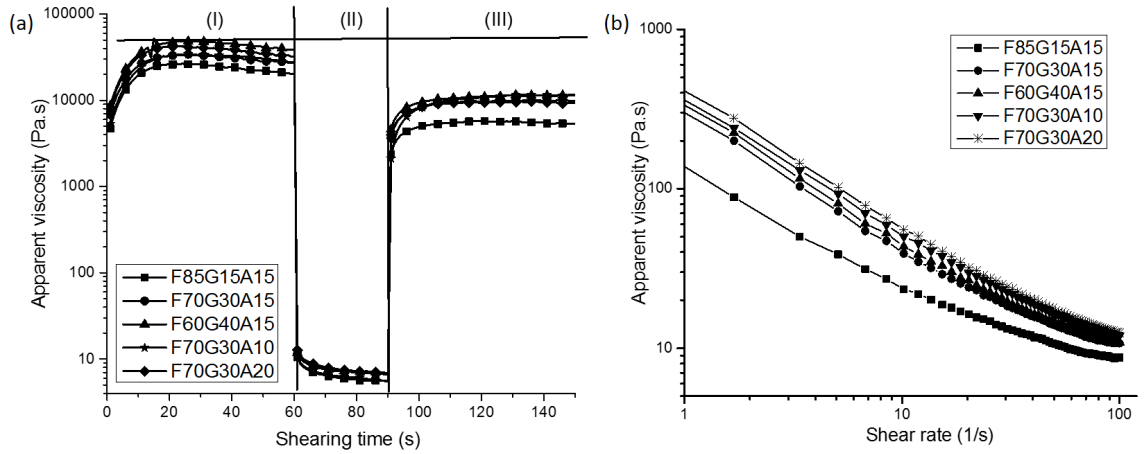

Fig. 5 Assessment of the prepared mixes for their (a) viscosity recovery and (b) shear thinning behaviours

The thixotropy index (A_{thix}) of the geopolymer mixes, listed in Table 4, increased with an increase in the amount of GGBS, which was an indication of the strong bonding due to the angular morphology of the GGBS particles. With the use of higher contents of GGBS that replaced FA, the rolling nature of spherical FA diminished, increasing the particle-to-particle interlocking. Increase in packing density could therefore explain the enhanced thixotropy observed in geopolymer mixes with high GGBS contents. Alternatively, the increase in the activator content from 10 to 20% reduced the A_{thix} value, which could be attributed to the weaker bonding between colloidal particles due to the plasticizing effect of silicates. Within these mixes, silicate anions could have adsorbed on the particle surfaces, increasing the inter particle distance [31], and hence A_{thix}. Considering that the main indented use for the mixes designed in this study were non-structural printed components requiring a strength of 25-30 MPa, mix F70G30A10 was selected for demonstrative 3D printing, as well as the further analysis of its mechanical properties and characterization of its phase formations and microstructure.

Table 4. Thixotropy index (A_{thix}) of geopolymer mixes at 300 RPM

F85G15A15	F70G30A15	F60G40A15	F70G30A10	F70G30A20
2.14	2.50	2.85	3.09	2.27

3.2 Print quality

Print quality refers to the properties of the 3D printed layers of a mix, such as their extrudability, dimensional conformity and shape effects at different print speeds and constant flow rate. Fig. 6(a) shows the results of the extrudability test of mix F70G30A10, which was continuously extruded without any breakage or discontinuity at a speed of 90 mm/sec for a total length of one meter. The speed of printing was confirmed by printing six straight lines at different speeds (Fig. 6(b)) and comparing the bead width (W) with the nozzle opening width (30 mm). As using a printing speed of 90 mm/sec led to an equivalent width of 30 mm, this speed was used in the subsequent printing of a 10-cm diameter cylinder (Fig. 6(c)) to indicate the feasibility of using the developed one-part geopolymer mixes in 3D printing applications.

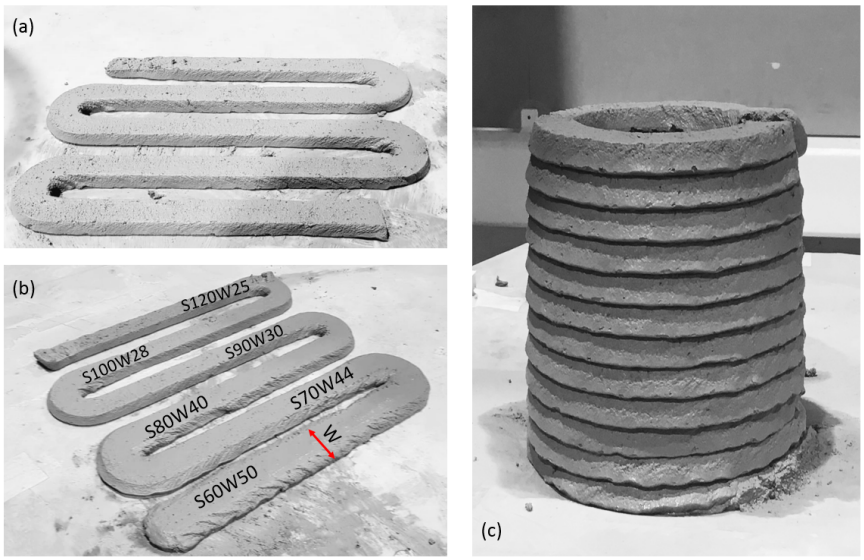

Fig. 6 Assessment of mix F70G30A10 for its (a) extrudability, (b) effect of printing speed and (c) 3D printing of 10 layers

3.3 Load carrying capacity

Load carrying capacity is one of the key properties of printable materials, commonly referred to as "buildability". Starting from mixing to setting, as the strength of the material progressively

grows, its measurement is highly necessary to predict the number of layers that can be safely deposited prior to structural collapse [35]. Fig. 7 shows the load carrying capacity of the selected one-part geopolymer mix. In the dormant period, the material strength was related to its green strength, followed by its hardened strength at 7, 14 and 28 days of ambient curing. For the F70G30A10 mix, the green strength was found to be 0.01 MPa, while the 28-day strength of the analysed samples reached 26.8 MPa. During 3D printing, green strength can be used as an indication of the number of layers that can be deposited without any significant deformation of the bottom layer, whereas the hardened strength indicates the point at which permanent failure can be expected. Unlike OPC-based mixes, the dormant period of the mixes prepared in this study was less than 30 minutes, thereby leading to an early strength development after 15 minutes of mixing due to the formation of aluminosilicate gel during the initial stage of the reaction. Such rapid strength development can be considered as an advantage in the concrete printing process, enabling the stacking up of the extruded layers without any need for accelerators. However, care must be taken during batch mixing to avoid the premature hardening of the bulk material for large scale printing applications. According to these findings, an in-line/continuous mixer is suggested for the simultaneous mixing and extrusion of one-part geopolymer mortars.

In some cases, where the low green strength of the extruded material may lead to difficulties in achieving higher buildability, accelerators can be added either during mixing or directly at the nozzle, so that the structural build-up rate can be accelerated to prevent the deformation of each layer. This reaction rate control mechanism has been discussed in recent studies [36, 37], where its importance and suitable admixtures that can help to meet the desired buildability without causing problems in the extrusion process were highlighted. Although most of the suggestions made in these studies were applicable to OPC-based binders, some of them may also be applied to geopolymer binders, depending on the type of raw materials and reaction mechanisms. Therefore, a further study on the use of admixtures to control the structural build-up of geopolymer mixes during 3D printing must be performed.

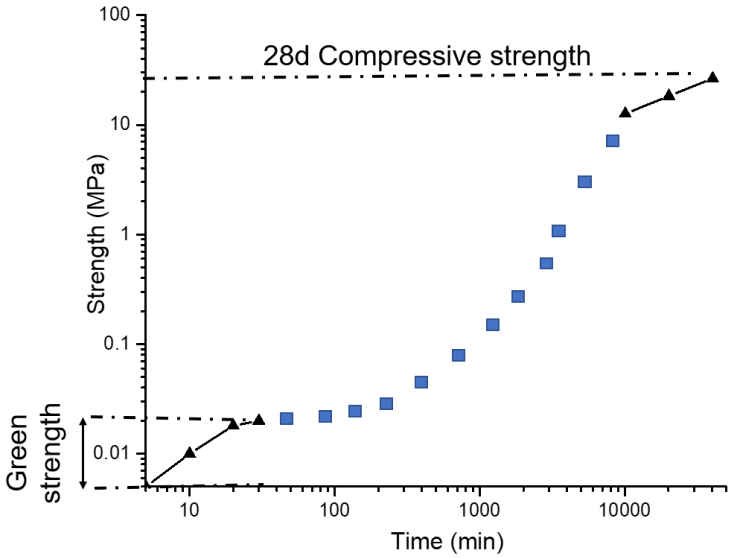

Fig. 7 Strength development curve of mix F70G30A10

(Note: black points were obtained experimentally, whereas blue points were illustratively added to obtain a continuous representation)

3.4 Mechanical properties of the 3D printed section

Directional mechanical strength is one of the inherent properties of the 3D printing process due to layer-wise manufacturing. In this regard, the most commonly used orthogonal directions F1, F2 and F3 are shown in Fig. 8(a). Accordingly, the average 28-day compressive strengths of 3D printed samples in F1, F2 and F3 directions were recorded as 28.3, 25.9 and 24.3 MPa, respectively (Fig. 8(b)). The compressive strengths of samples in F2 and F3 directions were comparable, while the strength in the F1 direction was highest among all. These values were relatively similar to the average strength of the mould cast samples, which was 26.5 MPa. Such anisotropy in mechanical property was previously mentioned in [38] for glass fiber reinforced geopolymer samples. However, it is not possible to state that this effect was observed in the different layer directions indicated in Fig. 8(a) since F1 and F3 had the same orientation. The difference in strength could be associated with the motion patterns of the material during the printing process. Accordingly, as the movement of the material through the system was in the direction shown in F1, it is possible that in that direction of movement, the particles were placed and compacted better than the other directions, thereby providing a higher compressive strength.

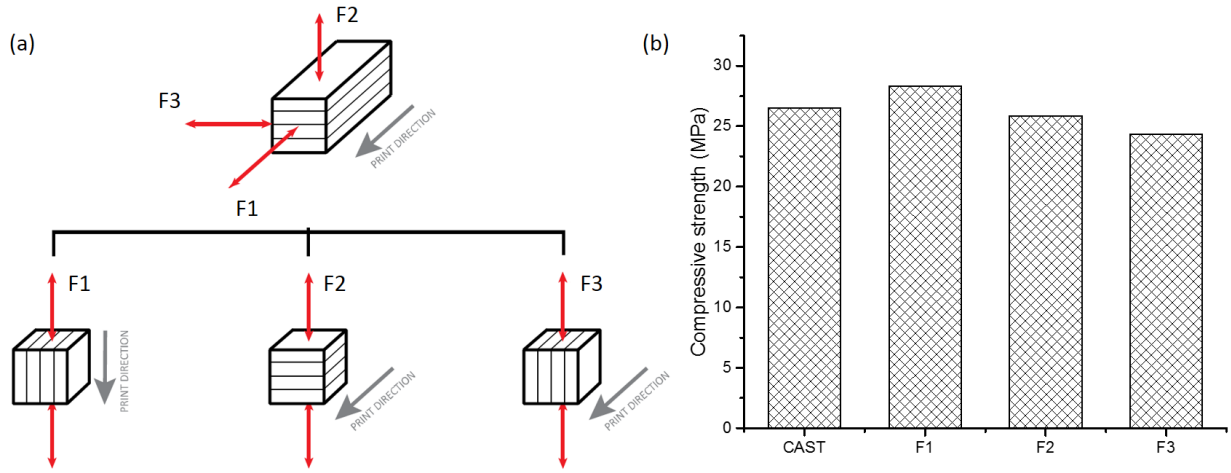

Fig. 8 Assessment of mix F70G30A10, showing its (a) schematic view of the three testing directions and (b) 28-day compressive strength of printed sections in comparison with mould casted specimens

3.5 Microstructural analysis via XRD and SEM

The microstructural analysis of mix F70G30A10 after 28 days of curing revealed the presence of aluminosilicate gel and unreacted FA and GGBS particles, as shown in Fig. 9. In both cured and uncured systems, a broad hump was observed. In the unreacted system, the hump located at around 20-30° 2θ represented the glassy portion contributed by FA and GGBS. The change in the hump between 15 and 30° 2θ, as shown in Fig. 10, indicated the formation of amorphous gel within mix F70G30A10. The potassium alumino-silicate gel (K-A-S-H) phase, identified at around 29.4° 2θ was the main reaction product in F70G30A10. Further quantification of this amorphous gel by Rietveld analysis, as described in [22], is shown in Table 5. The obtained results revealed that the amorphous phase comprised nearly 50% of the sample, which was comparatively less than what was reported in previous studies [21]. Since the mechanical performance of geopolymer systems depends on their amorphous gel content [2], this low amorphous (reaction) product formation could explain the relatively low compressive strength of mix F70G30A10.

Zeolites K (PDF# 022-0793) and Zeolite G (PDF# 019-0092) were identified as the secondary reaction products in mix F70G30A10, along with major crystalline phases such as quartz, mullite and gehlenite. The formation of zeolites could explain the initial hardening of geopolymer mixes, which enabled the printing of subsequent deposited layers during the 3D printing process. Unlike OPC, geopolymer binders gain green strength due to the formation of nanocrystalline zeolites, compacted by an amorphous gel. Therefore, the reaction associated mechanism needs to be tailored according to the deposition speed of each layer to avoid the premature failure or collapse of the printed structure. In this regard, further research can be carried out to control the zeolite production, which can significantly influence the structural built-up property necessary for the 3D printing of geopolymer mixes.

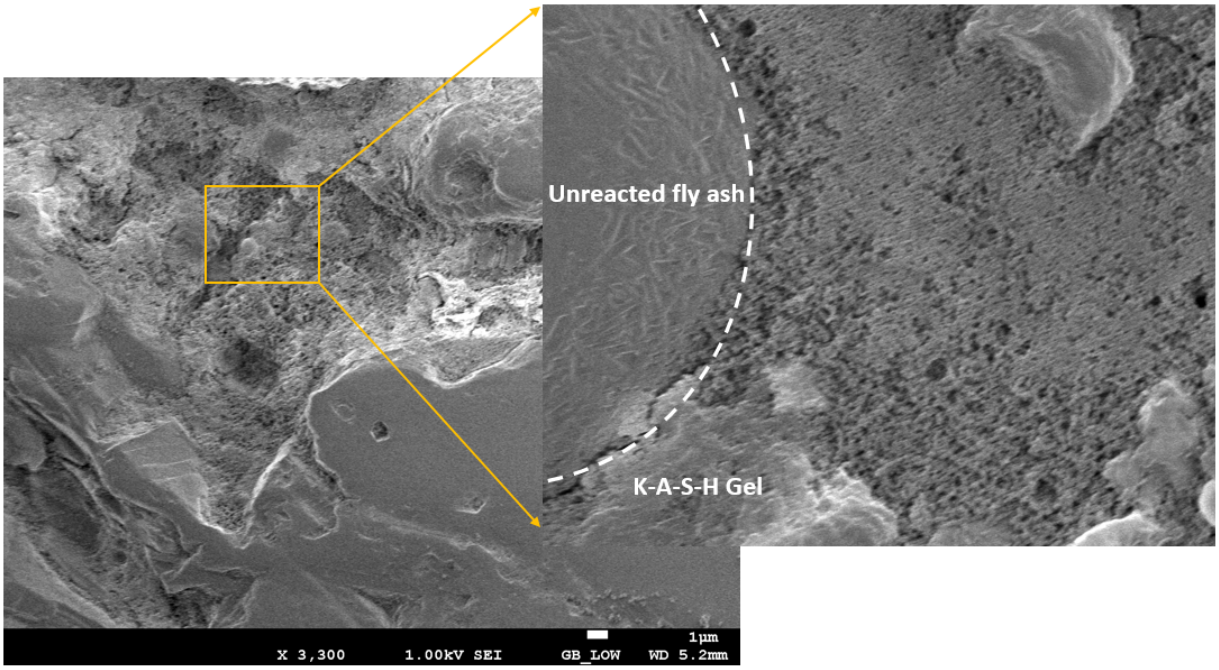

Fig. 9 SEM micrograph of mix F70G30A10 after 28 days of ambient curing

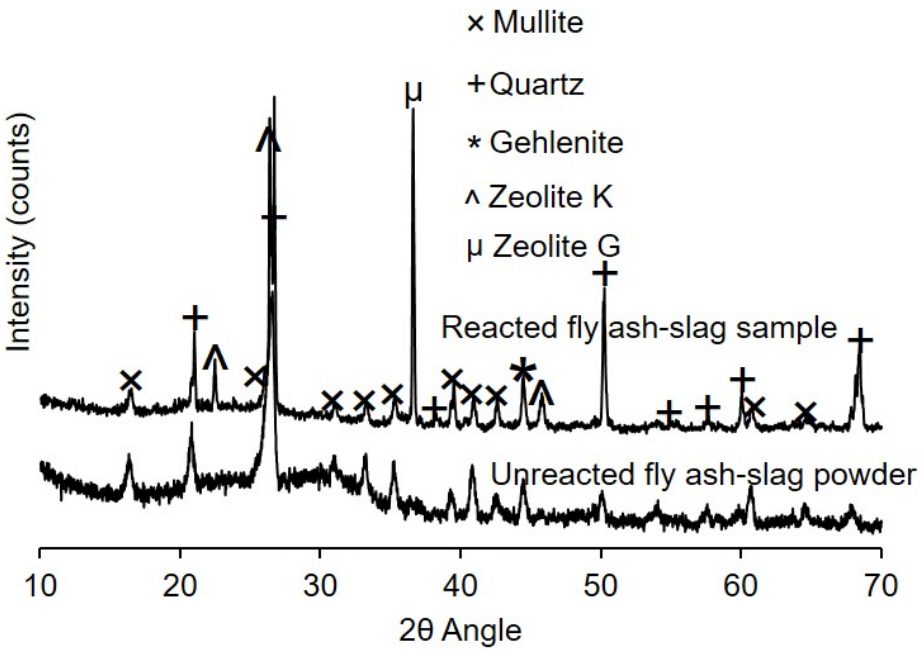

418

419 **Fig. 10** XRD patterns of unreacted FA-GGBS and mix F70G30A10

420

421 **Table 5.** Quantities of phases within unreacted FA-GGBS and mix F70G30A10 at 28 days

Compound	Unreacted FA-GGBS	Reacted FA-GGBS (F70G30A10)
Quartz	13.3	11.2
Mullite	25.0	10.2
Hematite	0.4	0.9
Magnetite	0.2	0.9
Rutile	0.2	0.2
Calcite	0.2	0.6
Gehlenite	1.2	0.1
Zeolite K	-	9.9
Zeolite G	-	13.9
Amorphous reaction content	59.6	52.1

422

423

424 **3.6 Environmental assessment**

425

The total energy and CO_2 emissions of one-part geopolymer samples are mainly a function of the amount of eCO_2 emissions and corresponding embodied energy of each component used within a particular mix design. Other factors contributing to the overall environmental impact include the energy required and eCO_2 emitted during the transport of raw materials and the construction (i.e. printing) process. As this study mainly focuses on the development of geopolymer mixes for the 3D printing of non-structural components, the main goal is to provide a quick comparison of the environmental impacts of these mixes with traditional OPC-based mixes. Accordingly, the environmental implications associated with the aggregates used in the mix design were not included in this comparison as both mixes (i.e. geopolymer and OPC-based) would include an equivalent amount of aggregates. Similarly, the transport of the raw materials to the production facility or the final product to site was not incorporated in the overall calculation of the environmental impacts, as these values were assumed to be similar for both scenarios.

The embodied energy and eCO_2 values used in this environmental assessment were 0.05 GJ and 0.027 tonne of eCO_2 per tonne of FA [41]; and 0.33 GJ and 0.113 tonne of eCO_2 per tonne of GGBS [42], respectively. As FA is a waste by-product obtained from coal burning power plants, some studies have considered it to have zero eCO_2 emissions. However, there are some environmental implications associated with its collection and transport, similar to other materials used in the mix design. In terms of the alkali activator, the composition of the activator and the associated production process have a significant impact on its CO_2 emissions. In this study, 1.0 tonne of eCO_2 per tonne of silicate was considered [43], which did not include the energy used during the extraction of raw materials, production and transport. According to the mix design used in the selected sample (F70G30A10), the total amount of eCO_2 was calculated to be around 0.15 tonne per tonne of binder (i.e. FA: 0.02 tonne, GGBS: 0.03 tonne and activator: 0.1 tonne). Considering that the eCO_2 and embodied energy associated with PC production are 0.90 tonne and 4.5 GJ per tonne of OPC [44], respectively, the eCO_2 of the geopolymer mix prepared in this study was around 83% lower.

Similar to the eCO_2 values, the amount of energy associated with the proposed geopolymer mix was calculated as 0.67 GJ per tonne of binder (i.e. FA: 0.04 GJ, GGBS: 0.1 GJ and activator: 0.54 GJ), which was around 15% of the embodied energy of an OPC-based sample. A closer look into

the individual contribution of the raw materials revealed the important role the activator played, which was around 81% of the total energy of the overall mix. Similar findings were revealed by previous studies [44, 45], where the advantage of using geopolymer mixes in comparison to OPC-based mixes in terms of environmental implications, were indicated. Considering that the two main binder components used in this study, FA and GGBS, are classified as by-products and therefore have very limited environmental impacts, a further optimization of the activator usage can have a notable impact in lowering the overall embodied energy and eCO_2 values associated with geopolymers. In this respect, alternative activators that are known to have lower environmental impacts can be utilized, thereby resulting in mixes that are even more sustainable, provided that the desired mechanical performance is maintained throughout the 3D printing process.

4. Conclusions

This study focused on the development of 3D printable one-part geopolymers that possess thixotropy property. The prepared mixes were evaluated for their feasibility to be used in digital construction. The followed approach included an assessment of thixotropy, static yield stress, viscosity and mechanical and microstructural properties, along with a comparison of the environmental impact with OPC-based mixes. The results emerging from this study can be summarized as follows:

- The developed geopolymer mixes could be printed as sections with a height of up to 300 mm by depositing consistent filaments without any noticeable deformation of the bottom layers.
- Yield stress, thixotropy as well as mechanical strength increased with increasing GGBS content due to the angular morphology and amorphous phases present in GGBS.
- The prepared mixes exhibited thixotropic behaviour with an ability of recovering 70-80% of their original viscosity within 60 seconds of extrusion. Therefore, the layers could be deposited in 60-second time intervals, without deforming the bottom layers.
- The printed geopolymers showed anisotropic mechanical performance when compared to the mould casted specimens due to the layer wise fabrication approach used in the concrete printing.

- The final product was found to contain potassium-aluminosilicate gel, which can explain the mechanical and microstructural development observed within the prepared samples.
- One-part geopolymers, an alternative green binder that is activated by solid activators, have the potential to result in lower environmental impacts than those associated with OPC-based mixes.

Overall, the findings revealed in this paper have provided new insights on the rheological properties of one-part geopolymers under the context of 3D concrete printing. As the precise control of material "fluidity" and "green strength" are essential in 3D printing, specific emphasis was given on the study of various mix designs that affected the rheology of geopolymer mortars. Further research should focus on establishing a deeper understanding of the reaction mechanisms to improve the mechanical performance of the prepared formulations. This will enable the end user to tailor the rheology with the inclusion of proper additives in line with the desired outcome, as depicted in Fig. 11.

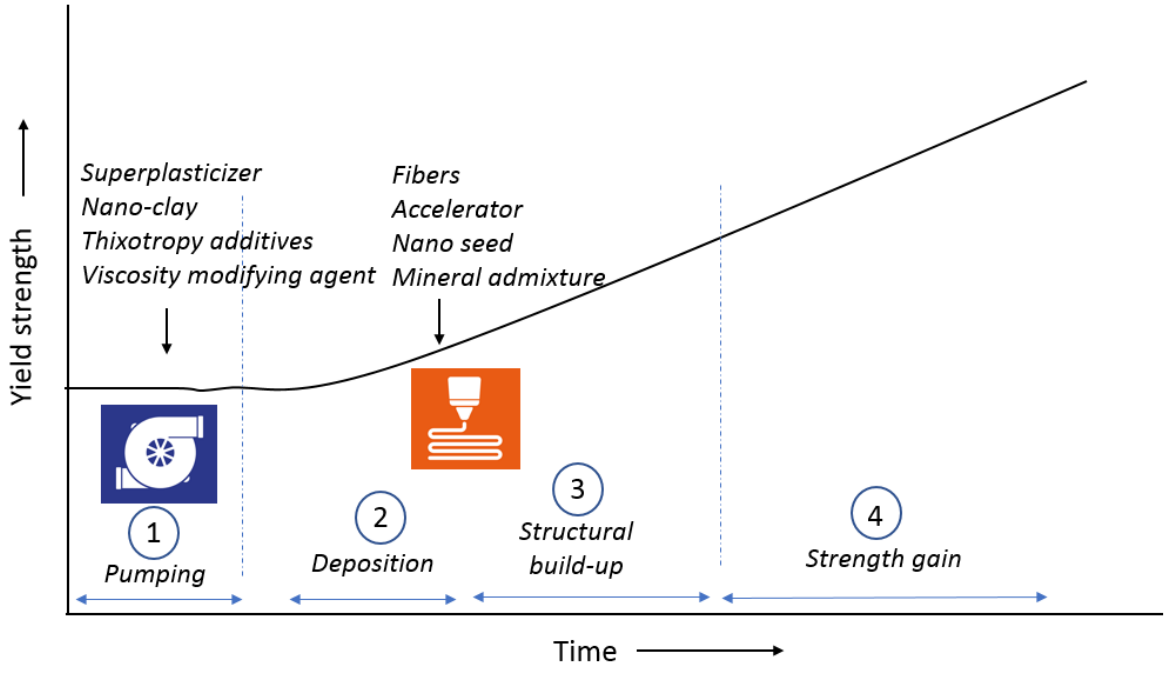

Fig. 11 Schematic representation of the strength development curve with the use of different additives at various stages of 3D concrete printing

Acknowledgements

The authors would like to acknowledge Sembcorp Architects & Engineers Pte. Ltd. and National Research Foundation (NRF) Singapore for their funding and support in this research project.

References

1. Davidovits, J., 1991. Geopolymers: inorganic polymeric new materials. Journal of Thermal Analysis and calorimetry, 37(8), pp.1633-1656.

2. Van Deventer, J.S.J., Provis, J.L., Duxson, P. and Lukey, G.C., 2007. Reaction mechanisms in the geopolymeric conversion of inorganic waste to useful products. Journal of Hazardous Materials, 139(3), pp.506-513.

3. Luukkonen, T., Abdollahnejad, Z., Yliniemi, J., Kinnunen, P. and Illikainen, M., 2018. Comparison of alkali and silica sources in one-part alkali-activated blast furnace slag mortar. Journal of Cleaner Production, 187, pp.171-179.

4. Adesanya, E., Ohenoja, K., Luukkonen, T., Kinnunen, P. and Illikainen, M., 2018. One-part geopolymer cement from slag and pretreated paper sludge. Journal of Cleaner Production, 185, pp.168-175.

5. Ye, N., Yang, J., Liang, S., Hu, Y., Hu, J., Xiao, B. and Huang, Q., 2016. Synthesis and strength optimization of one-part geopolymer based on red mud. Construction and Building Materials, 111, pp.317-325.

6. Choo, H., Lim, S., Lee, W. and Lee, C., 2016. Compressive strength of one-part alkali activated fly ash using red mud as alkali supplier. Construction and Building Materials, 125, pp.21-28.

7. Luukkonen, T., Abdollahnejad, Z., Yliniemi, J., Kinnunen, P. and Illikainen, M., 2017. One-part alkali-activated materials: A review. Cement and Concrete Research. 103 (2018) 21–34

8. Buswell, R.A., de Silva, W.L., Jones, S.Z. and Dirrenberger, J., 2018. 3D printing using concrete extrusion: a roadmap for research. Cement and Concrete Research.

9. Khoshnevis, B., 2004. Automated construction by contour crafting—related robotics and information technologies. Automation in construction, 13(1), pp.5-19.

10. Wangler, T., Lloret, E., Reiter, L., Hack, N., Gramazio, F., Kohler, M., Bernhard, M., Dillenburger, B., Buchli, J., Roussel, N. and Flatt, R., 2016. Digital concrete: opportunities and challenges. RILEM Technical Letters, 1, pp.67-75.

11. Le, T.T., Austin, S.A., Lim, S., Buswell, R.A., Gibb, A.G. and Thorpe, T., 2012. Mix design and fresh properties for high-performance printing concrete. Materials and structures, 45(8), pp.1221-1232.

12. Kazemian, A., Yuan, X., Cochran, E. and Khoshnevis, B., 2017. Cementitious materials for construction-scale 3D printing: Laboratory testing of fresh printing mixture. Construction and Building Materials, 145, pp.639-647.

13. Feng, P., Meng, X., Chen, J.F. and Ye, L., 2015. Mechanical properties of structures 3D printed with cementitious powders. Construction and Building Materials, 93, pp.486-497.

14. Panda, B., Paul, S.C., Hui, L.J., Tay, Y.W.D. and Tan, M.J., 2017. Additive manufacturing of geopolymer for sustainable built environment. Journal of Cleaner Production, 167, pp.281-288.

15. Roussel, N., 2018. Rheological requirements for printable concretes. Cement and Concrete Research.

16. Xia, M. and Sanjayan, J., 2016. Method of formulating geopolymer for 3D printing for construction applications. Materials & Design, 110, pp.382-390.

17. Panda, B. and Tan, M.J., 2018. Experimental study on mix proportion and fresh properties of fly ash based geopolymer for 3D concrete printing. Ceramics International, 44(9), pp.10258-10265.

18. Tay, Y.W.D., Panda, B., Paul, S.C., Noor Mohamed, N.A., Tan, M.J. and Leong, K.F., 2017. 3D printing trends in building and construction industry: a review. Virtual and Physical Prototyping, 12(3), pp.261-276.

19. Panda, B., Paul, S.C., Mohamed, N.A.N., Tay, Y.W.D. and Tan, M.J., 2018. Measurement of tensile bond strength of 3D printed geopolymer mortar. Measurement, 113, pp.108-116.

20. Bos, F., Wolfs, R., Ahmed, Z. and Salet, T., 2016. Additive manufacturing of concrete in construction: potentials and challenges of 3D concrete printing. Virtual and Physical Prototyping, 11(3), pp.209-225.

21. Singh, G.B. and Subramaniam, K.V., 2016. Quantitative XRD study of amorphous phase in alkali activated low calcium siliceous fly ash. Construction and Building Materials, 124, pp.139-147.

22. Singh, G.B. and Subramaniam, K.V., 2018. Characterization of Indian fly ashes using different experimental techniques. Indian Concrete Journal, 92(3), pp.10-23.

23. Davidovits, J., 2008. Geopolymer chemistry and applications. Geopolymer Institute.

24. Nematollahi, B., Sanjayan, J. and Shaikh, F.U.A., 2015. Synthesis of heat and ambient cured one-part geopolymer mixes with different grades of sodium silicate. Ceramics International, 41(4), pp.5696-5704.

25. Ma, S., Qian, Y., & Kawashima, S. 2018. Experimental and modeling study on the non-linear structural build-up of fresh cement pastes incorporating viscosity modifying admixtures. Cement and Concrete Research, 108, pp.1-9.

26. Lim, J.H., Panda, B. and Pham, Q.C., 2018. Improving flexural characteristics of 3D printed geopolymer composites with in-process steel cable reinforcement. Construction and Building Materials, 178, pp.32-41.

27. ASTM C109/C109M-13, Standard Test Method for Compressive Strength of Hydraulic Cement Mortars (Using 2-in. or [50-mm] Cube Specimens), ASTM Committee C01, West Conshohocken, PA 19428-2959, United States, 2013, p. 10.

28. Voigt, T., Malonn, T. and Shah, S.P., 2006. Green and early age compressive strength of extruded cement mortar monitored with compression tests and ultrasonic techniques. Cement and Concrete Research, 36(5), pp.858-867.

29. Deb, P.S., Nath, P. and Sarker, P.K., 2014. The effects of ground granulated blast-furnace slag blending with fly ash and activator content on the workability and strength properties of geopolymer concrete cured at ambient temperature. Materials & Design (1980-2015), 62, pp.32-39.

30. Cheah, C.B., Samsudin, M.H., Ramli, M., Part, W.K. and Tan, L.E., 2017. The use of high calcium wood ash in the preparation of Ground Granulated Blast Furnace Slag and Pulverized Fly Ash geopolymers: A complete microstructural and mechanical characterization. Journal of Cleaner Production, 156, pp.114-123.

31. Kashani, A., Provis, J.L., Qiao, G.G. and van Deventer, J.S., 2014. The interrelationship between surface chemistry and rheology in alkali activated slag paste. Construction and Building Materials, 65, pp.583-591.

32. Collins, F. G., & Sanjayan, J. G. 1999. Workability and mechanical properties of alkali activated slag concrete. Cement and concrete research, 29(3), 455-458.

598 33. Puertas, F., Martı´nez-Ramı´rez, S., Alonso, S., & Vazquez, T. 2000. Alkali-activated fly
599 ash/slag cements: strength behaviour and hydration products. Cement and Concrete Research,
600 30(10), 1625-1632.
601 34. Alonso, M.M., Gismera, S., Blanco, M.T., Lanzón, M. and Puertas, F., 2017. Alkali-
602 activated mortars: Workability and rheological behaviour. Construction and Building Materials,
603 145, pp.576-587.
604 35. Wolfs, R.J.M., Bos, F.P. and Salet, T.A.M., 2018. Early age mechanical behaviour of 3D
605 printed concrete: Numerical modelling and experimental testing. Cement and Concrete Research,
606 106, pp.103-116.
607 36. Reiter, L., Wangler, T., Roussel, N. and Flatt, R.J., 2018. The role of early age structural
608 build-up in digital fabrication with concrete. Cement and Concrete Research.
609 37. Marchon, D., Kawashima, S., Bessaies-Bey, H., Mantellato, S. and Ng, S., 2018. Hydration
610 and rheology control of concrete for digital fabrication: Potential admixtures and cement
611 chemistry. Cement and Concrete Research.
612 38. Panda, B., Paul, S.C. and Tan, M.J., 2017. Anisotropic mechanical performance of 3D
613 printed fiber reinforced sustainable construction material. Materials Letters, 209, pp.146-149.
614 39. Criado, M., Fernández-Jiménez, A., De La Torre, A.G., Aranda, M.A.G. and Palomo, A.,
615 2007. An XRD study of the effect of the SiO_2/Na_2O ratio on the alkali activation of fly ash. Cement
616 and concrete research, 37(5), pp.671-679.
617 40. Hajimohammadi, A. and van Deventer, J.S., 2017. Characterisation of one-part geopolymer
618 binders made from fly ash. Waste and Biomass Valorization, 8(1), pp.225-233.
619 41. Jamieson, E., McLellan, B., Van Riessen, A., & Nikraz, H. 2015. Comparison of embodied
620 energies of Ordinary Portland Cement with Bayer-derived geopolymer products. Journal of
621 Cleaner Production, 99, pp. 112-118.
622 42. Habert G., d'Espinose de Lacaillerie J.B., Roussel N., 2011. An environmental evaluation of
623 geopolymer based concrete production: reviewing current research trends, Journal of Cleaner
624 Production 19, pp. 1229-1238.
625 43. Ouellet-Plamondon C., Habert G., 2014 Life Cycle Assessment (LCA) of alkali-activated
626 cements and concretes, Handbook of Alkali Activated Cements, Mortars and Concretes.
627 Woodhead Publishing

628 44. Turner L. K., Collins F. G., 2013 Carbon dioxide equivalent (CO2-e) emissions: A comparison
629 between geopolymer and OPC cement concrete, Construction and Building Materials 43, pp.125–
630 130
631 45. McLellan B. C., Williams R. P., Lay J., van Riessen A., Corder G. D., 2011 Costs and carbon
632 emissions for geopolymer pastes in comparison to ordinary Portland cement, Journal of Cleaner
633 Production 19, pp.1080-1090